Meteorol. Z. (Contrib. Atm. Sci.), Vol. 33 (2024), 285–292
Published online August 13, 2024

Open Access Article
Atmospheric Dynamics

Characteristics of rain cells over the northwest Pacific warm pool

Ping Ye[1], Aoqi Zhang[2,3,*]

[1] Zhongshan Meteorological Service, Zhongshan 528400, China
[2] School of Atmospheric Sciences and Key Laboratory of Tropical Atmosphere-Ocean System, Ministry of Education, Sun Yat-Sen University, Zhuhai 519082, China
[3] Southern Marine Science and Engineering Guangdong Laboratory (Zhuhai), Zhuhai 519082, China
* Corresponding author: zhangaoq3@mail.sysu.edu.cn

With 6 figures and 1 table

Abstract: The importance of precipitation morphology has been emphasized by recent studies. However, the specific morphological characteristics of rain cells (RCs) and their impact on rainfall intensity over the oceans remain unclear. In this study, using 15-year observations from Tropical Rainfall Measurement Mission (TRMM) Precipitation Radar (PR), more than 600 thousand RCs in the northwest Pacific warm pool were identified and approximated by rectangle. The results showed that the horizontal scale of RCs was negatively correlated with their occurrence frequency, while there was a logarithmic correlation between the length and width of the approximated rectangle. The morphology of RCs presented huge zonal differences but small meridional differences over the study region. RCs had larger scale, narrower 2-D shape, and slender 3-D shape in the southern region compared with ones in the northern region. Precipitation intensity generally increased with the enlargement of the horizontal scale. The relationships between precipitation intensity and shape of RCs were very complex. Moderate shape of RCs had the weakest precipitation, whereas 2-D narrower or 3-D slender RCs had the strongest precipitation. The results would be helpful for monitoring and predicting precipitating clouds over the oceans.

Keywords: Northwest Pacific warm pool, rain cells, TRMM PR, morphology, rainfall intensity

1 Introduction

The northwest Pacific (NWP) is the warmest ocean over the world, constructing a key supplier of atmospheric heat, and is named as the "warm pool" (Barlow et al. 2002; Park et al. 2012). The air-sea interaction is very intense over the NWP warm pool, thus convective activities are quite frequent. The energy released by those convections supports the Walker circulation and even the atmospheric circulation of the whole northern hemisphere (Cornejo-Garrid & Stone 1977; Jiang & Zhu 2020). In these years, many researches showed that the thermal regime of the NWP is closely related to El Niño–Southern Oscillation (ENSO) events, making it a key region for studying global climate change (Basconcillo et al. 2021; Zhang et al. 2022a).

Precipitation activities are very important in studying atmospheric circulation as well as climate change. The precipitation in the NWP is inextricably bound to the thermal regime of NWP and even all the world (Luna & Korup 2022). Based on the Tropical Ocean Global Atmosphere-Coupled Ocean Atmosphere Response Experiment (TOGA-COARE), Li et al. (1998) found that heavy precipitation over the NWP can cause sharp decrease of salinity as well as sea surface temperature (SST). Rain cells (RCs) are event-scale components of precipitation, often identified by grouping connected precipitation pixels, and has attracted much attention in recent studies (Zhang & Fu 2018; Kumar et al. 2019; Zhang et al. 2022b). The studies on morphology and physics of RCs are helpful for knowledges on water cycle, energy budget, and climate change (Nesbitt et al. 2000; Fu et al. 2020).

Using data from ground-based radars, scholars have launched numerous studies on RCs (Capsoni et al. 1987; Feral et al. 2000). Initially, most studies still focused on the physical features of RCs, such as precipitation intensity, echo-top height, and horizontal diffusion of precipitation (Gagin et al. 1986; Tsonis et al. 1996; Kawamura et al. 1996, 1997). As time went by, the horizontal scale and other morphological characteristics drew more attention. Sauvageot et al. (1999) used rounds to describe the shape of RCs, and listed the distribution features of the rounds' diameter. Feral et al. (2000) further quantified the 2-D shape of RCs using major and

DOI: 10.1127/metz/2024/1212
Gebrüder Borntraeger Science Publishers, Stuttgart, www.borntraeger-cramer.com

minor axis of ellipse. Begum & Otung (2009) investigated the size distribution of RCs in the United Kingdom.

However, since ground-based radars are highly limited by the terrain, they cannot be used to study RCs over the ocean or other desolate place. Some scientists put forward a method that using satellite altimeter to retrieve the precipitation structure of RCs over the ocean (Quartly 1998; Tournadre 1998). Nevertheless, the swath of satellite altimeter is too narrow to be used in practice. Fortunately, the successful launch of Tropical Rainfall Measurement Mission (TRMM) Precipitation Radar (PR) provides a favorable opportunity for detailed studies on the precipitation over tropical and subtropical ocean. Adler et al. (2000) studied the tropical rainfall distributions using TRMM PR together with other satellite and rain gauge information. Liu & Zipser (2013) established a dataset of RCs from TRMM PR, and investigated the regional variation of RC morphology in the tropics and subtropics. Yokoyama & Takayabu (2012) used Liu's dataset, and found that rainfalls are dominated by tall unorganized systems and very tall organized systems in high-SST regions including the NWP.

The above work laid a good foundation for the research on RCs over the ocean. However, the morphological characteristics of RCs and their impact on precipitation features remain unclear. Most previous studies use ellipse to approximate the shape of RCs, but ellipse cannot contain all precipitation pixels within RCs. Besides, RCs may be truncated by TRMM PR swaths, which lead to inaccurate morphological information (Nesbitt et al. 2006). In this work, following Fu et al. (2020), the shape of RCs is approximated by minimum bounding rectangles, and the truncated rectangular are wiped out. We aim to investigate the morphological and physical features of RCs, as well as their correlations over the NWP.

2 Data and method

2.1 Data and sample size

Precipitation datasets used in this work are derived from TRMM PR. PR is the first space-borne Ku-band (13.8 GHz) precipitation radar. It has a narrow swath of 220 km with a horizontal resolution of 4.3 km (5 km after a boost in August 2001) and a vertical resolution of 250 m. The sensitivity of PR is 17 dBZ, which equivalents to rain rate of about 0.4 mm h^{-1} (Kummerow et al. 1998). We used the TRMM PR level-2 product 2A25, in which the corrected reflectivity, rain rate, and rain type are provided. Additionally, we also employed echo-top height, which is defined as the top of highest three continuous layers with reflectivity larger than 17 dBZ.

We identified RCs following the method of Fu et al. (2020). RCs consist of contiguous PR 2A25 pixels with near-surface rain rate lager than 0.4 mm h^{-1}. The shape of RC is approximated by the minimum bounding rectangle. The main parameters of the RC product will be shown in the section 2.2 together with a RC case. Two types of RCs are wiped out in this paper. One is RCs truncated by PR swath, the other is that consisted of four or less PR pixels.

The study region of NWP warm pool is showed in Fig. 1, and the study period is all year round from 1998 to 2012. Significant number of RCs were statistically studied in this work (Fig. 1a). For each 0.5°×0.5° grid, the number of RCs is about 250–600. The northern field of the northwest Pacific is often influenced by the subtropical high with less frequent precipitation. The sample size of RCs was averagely 275 over the northern portion of the NWP, while it was more than 500 over the southern portion of NWP. In addition, the differences between the SST and sunlight are also responsible for the zonal difference of RC sample size.

The spatial distributions of average near-surface rain rate are presented as Fig. 1b, with obvious regional differences. For the northern portion of NWP, the average rainfall was as weak as less than 2.1 mm h^{-1}, whereas it was 2.3 mm h^{-1} and 2.5 mm h^{-1} for the southeastern and southwestern portion, respectively. The zonal difference in rainfall patterns (between the northern and southern portions) may be due to the combined effects of SST and subtropical high. Specifically, warmer SSTs over the southern portion may enhance rainfall frequency and intensity, while the subtropical high (tend to occur in the northern portion and surroundings) may suppress rainfall in the northern region (Chen et al. 2020). The meridional difference between the southwestern and southeastern portion should be resulted from the differences of SST (Fig. 1c).

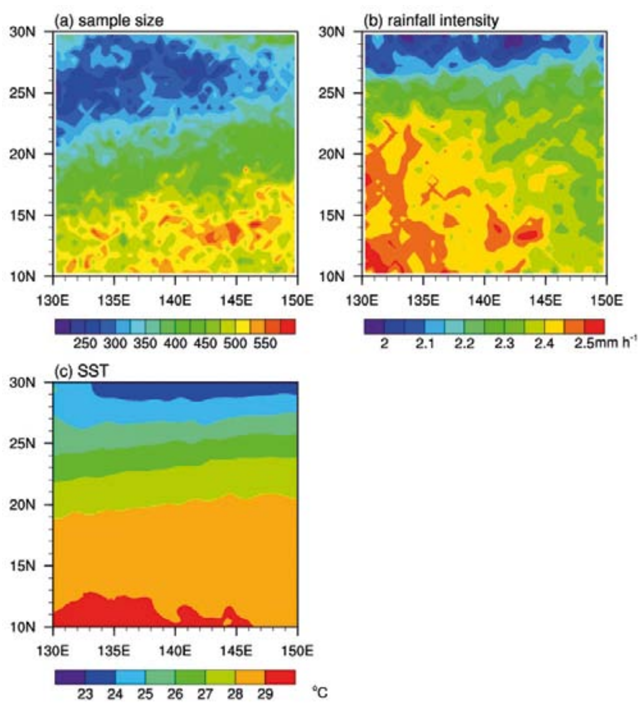

Fig. 1. Horizontal distributions of (a) RC sample size and (b) average rainfall intensity detected by TRMM PR, and (c) ERA5 average SST during the study period of 1998–2012.

2.2 Definition of morphological parameters

Fig. 2 shows a RC case over the southern portion of NWP. Three prominent morphological features of the RC are shown in this figure. Firstly, the RC example strides over six degrees of longitude and five degrees of latitude, indicating that it is large in scale. Secondly, the 2-D morphology of the RC and its minimum bounding rectangle are very narrow. In fact, large RCs detected by PR are usually very narrow under the restrictions of PR swath. Lastly, a lot of blank area besides RC pixels is shown in the rectangle. The proportion of blank area indicates the similarity of RC and the minimum bounding rectangle, also referred as beam filling effect in previous studies (Chen et al. 2021).

To describe the morphology of RC in a more efficient way, several parameters are defined following Fu's work (Fu et al. 2020). These parameters are listed in Tab. 1. The impact of three main variables, including L, α, and γ_{av}, on precipitation intensity was investigated in this work. L indicates the horizontal scale of RC (1-D shape). α shows the 2-D shape of RC with value range from 0–1. Small α indicates a narrow shape while large α indicates a wide shape. γ_{av} is the 3-D shape of RC. Small γ_{av} indicates a slender 3-D shape while large γ_{av} indicates a flat 3-D shape.

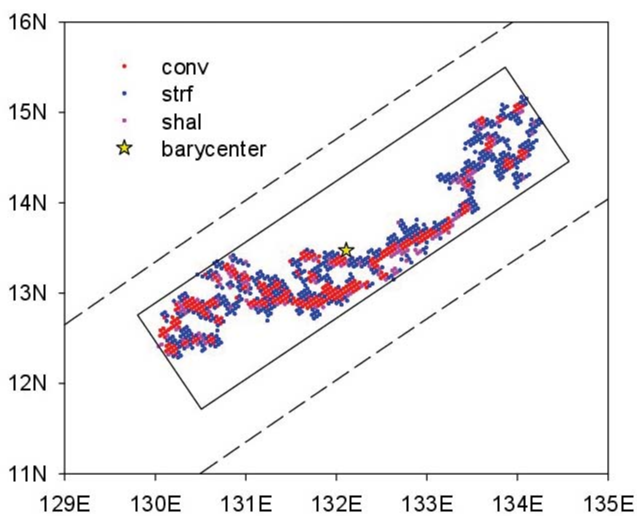

Fig. 2. A RC case detected by TRMM PR at 13:32 UTC 30 July 2011 over the NWP. The dash line is PR swath and the solid rectangle represents the minimum bounding rectangle.

3 Results

Firstly, we reviewed the precipitation features of RCs over the NWP. The probability density distributions (PDFs) of the average and maximum near-surface rain rate of RCs are shown in Fig. 3a–3b. Specifically, the average rain rate were calculated by averaging the rain rate of all pixels within the RC. Both presented a skew normal distribution, with peaks at 1.75 mm h^{-1} and 2.5 mm h^{-1} for average and maximum rain rate, respectively. There were 39.4% (22.5%) RCs with average (minimum) near-surface rain rate smaller than the peak. Comparing to the previous work on the precipitation of tropical and subtropical ocean (Liu et al. 2013), it is found that the maximum rainfall of RC was larger than the convective rain rate, whereas the average rainfall was between the rain rate of convective and stratiform precipitation.

Fig. 3c & 3d shows the PDFs of scale parameters L and S. It is generally concluded that the proportion of RC decreased shapely with the increase of horizontal scale. There were about 50% RCs with L (S) smaller than 20 km (100 km^2), whereas only 10% RCs with L (S) larger than 50 km (400 km^2). The PDF patterns of RC scale over the NWP was similar to the global average, while the proportion of large RCs was smaller over the NWP (Fu et al. 2020).

The PDFs of 2-D shape (α) and beam filling ratio (β) are shown in Fig. 3e & 3f. The PDF of α peaked at 0.6 with a value of 8%. Around 10% RCs had a α smaller than 0.4, whereas 35% RCs had a α larger than 0.7. The PDF of β peaked at 0.58 with a value of 20%. Less than 20% RCs had a β larger than 0.58.

The PDFs of echo-top height and 3-D shape are shown in Fig. 3g–3j. Both the average and maximum ones are given. The PDF of maximum echo-top height showed a bimodal distribution ranging from 0 to 16 km, with peaks at 3.5 and 5.5 km, respectively. The bimodal structure of echo-top height over the NWP was also pointed out by pixel-scale work in Thatcher et al. (2012). The average echo-top height of RCs ranged from 0 to 10 km with unique peak at 3 km.

Table 1. Definition of main morphological parameters and value of the case.

Variable	Definition	Value of the case in Fig. 2
L	Length of the minimum bounding rectangle	539.17 km
W	Width of the minimum bounding rectangle	144.15 km
α	2-D shape of RC, calculated by W/L	0.268
S	Area of the total precipitation pixels of RC	18762 km^2
β	Rate of S to the area of the minimum bounding rectangle	0.241
H_{av}	Average echo-top height of RC	4.72 km
γ_{av}	3-D shape of RC, calculated by $2H_{av}/(L+W)$	0.014

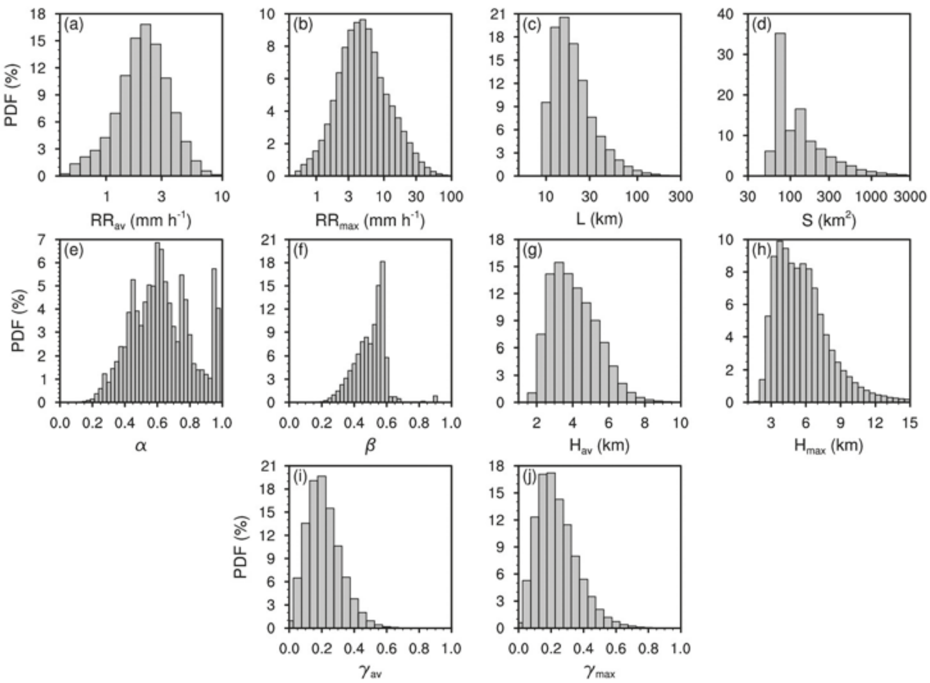

Fig. 3. PDFs of (a) average near-surface rain rate RR_{av}, (b) maximum near-surface rain rate RR_{max}, (c) length L, (d) area S, (e) 2-D shape α, (f) beam filling ratio β, (g) average echo-top height H_{av}, (h) maximum echo-top height H_{max}, (i) 3-D shape γ_{av}, and (j) γ_{max} for RCs over the NWP.

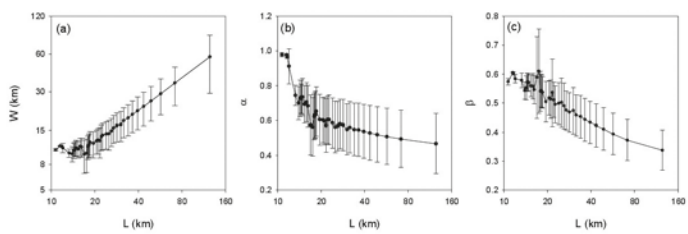

Fig. 4. Correlations between L and (a) W, (b) α, and (c) β for RCs over the NWP.

The patterns of the PDFs of average and minimum 3-D shape were quite similar (Fig. 3i & 3j). Both ranged from 0 to 0.8 with a peak at 0.2.

The correlations between L and other 1-D or 2-D shape parameters are showed in logarithmic coordinates in Fig. 4. The correlations showed two different stages depending on the value of L. When L was smaller than 20 km (indicating the total pixels of RC less than 16), W and β hardly changed with L and thus α sharply decreased with L. When L was larger than 20 km, there existed a log-linear correlation between W and L with a slope of 0.62 (Fig. 4a); α decreased slowly with L from 0.6 at 20 km to 0.5 at 100 km (Fig. 4b); β decreased shapely with L, showing more non-precipitation area within the minimum bounding rectangle (Fig. 4c). The results of Fig. 4c were similar to the statistics of all tropical and subtropical oceans (Fu et al. 2020).

To study the relationships between horizontal scale and rainfall intensity of RCs over the NWP, RCs were divided into three classes according to L, including small-scale RCs with $L < 20$ km, medium-scale RCs with $L \geq 20$ km and < 50 km, and large-scale RCs with $L \geq 50$ km.

The horizontal distributions of occurrence frequency for the three classes of RCs are shown in Fig. 5a–5c. Generally, the occurrence frequency of small RCs was the largest, followed by medium-scale RCs, and the smallest for large RCs. There was significant zonal difference for ratio distribution

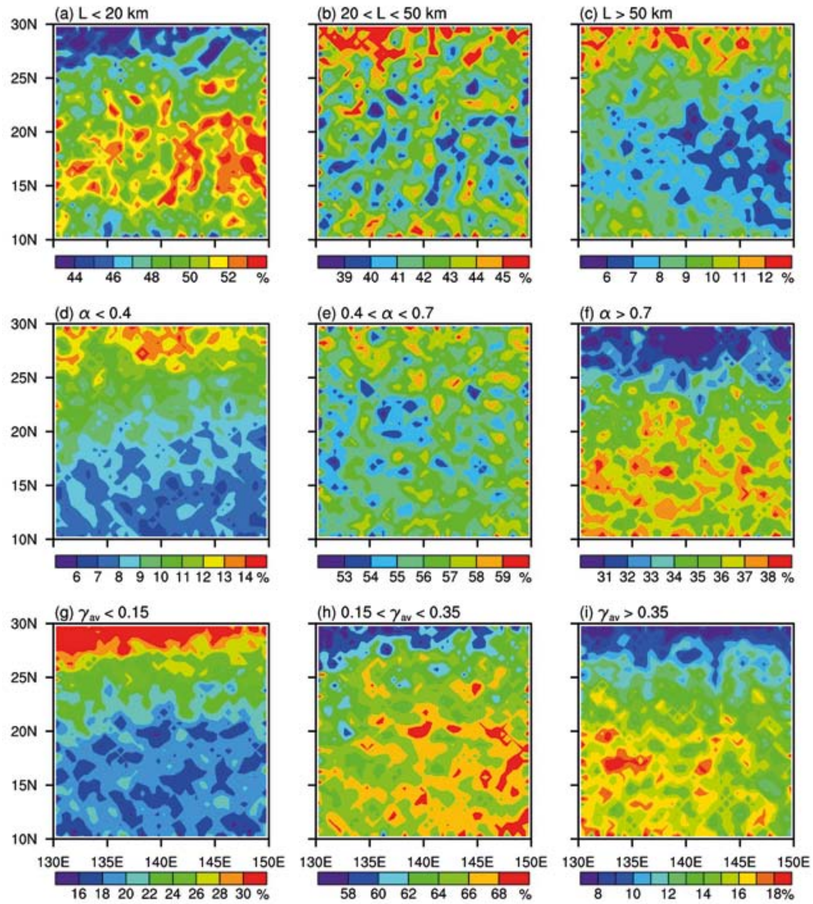

Fig. 5. Horizontal distributions of occurrence frequency for RCs divided by (a–c) scale L, (d–f) 2-D shape α, and (g–i) 3-D shape γ_{av} over the NWP.

of each class. The occurrence frequency of small RCs was about 50% over the southern portion, whereas less than 45% over the northern portion of NWP (Fig. 5a). The occurrence frequency of large RCs was about 7% over the southern portion while about 12% over the northern portion (Fig. 5c). The results showed that RCs over the northern portion of NWP had a higher potential to develop larger. We suggest it was related to that more warm-cloud precipitation occurs over the southern portion of NWP.

Fig. 6a–6c shows the spatial distributions of average near-surface rain rate for the three types of RCs divided by L. The distribution patterns of the three different classes of RCs were similar to the total RCs, with the strongest rain rate over the southwestern portion (Fig. 1b). The average near-surface rain rate was about 1.5–2.2 mm h^{-1}, 2–2.7 mm h^{-1}, and 2.6–3.8 mm h^{-1} for small, medium-scale, and large RCs, respectively. The precipitation intensity increased with L, which agrees to the previous studies (Tsonis et al. 1996).

RCs were also classified into three classes of RCs according to the 2-D shape α, including narrow RCs with α smaller than 0.4, medium 2-D shape RCs with α between 0.4 and 0.7, and wide RCs with α larger than 0.7. The horizontal distributions of their occurrence frequency are drawn in Fig. 5d–5f with dramatic zonal differences for narrow and wide RCs. About 8% RCs over the southern portion of NWP were narrow RCs, while the ratio was 13% over the northern portion (Fig. 5d). 37% RCs over the southern portion whereas 31% RCs over the northern portion were wide RCs (Fig. 5f). These zonal differences can be explained by the zonal difference of RC scale and the relationship between scale and 2-D shape.

The horizontal distributions of the average near-surface rain rate for the three types of RCs are showed in Fig. 6d–6f. Narrow RCs, which often initiated from MCSs, were companied with the heaviest rain rate (Fig. 6d). The medium 2-D-shape RCs had the weakest precipitation, indicating the most unfavorable 2-D-shape of heavy precipitation over the NWP. The relationships between α and rainfall intensity were very different from the Tibetan Plateau, where narrow RCs had the weakest precipitation (Chen et al. 2021). Therefore, it is of great importance of carry out regional studies of the relationship between RC morphology and physical features.

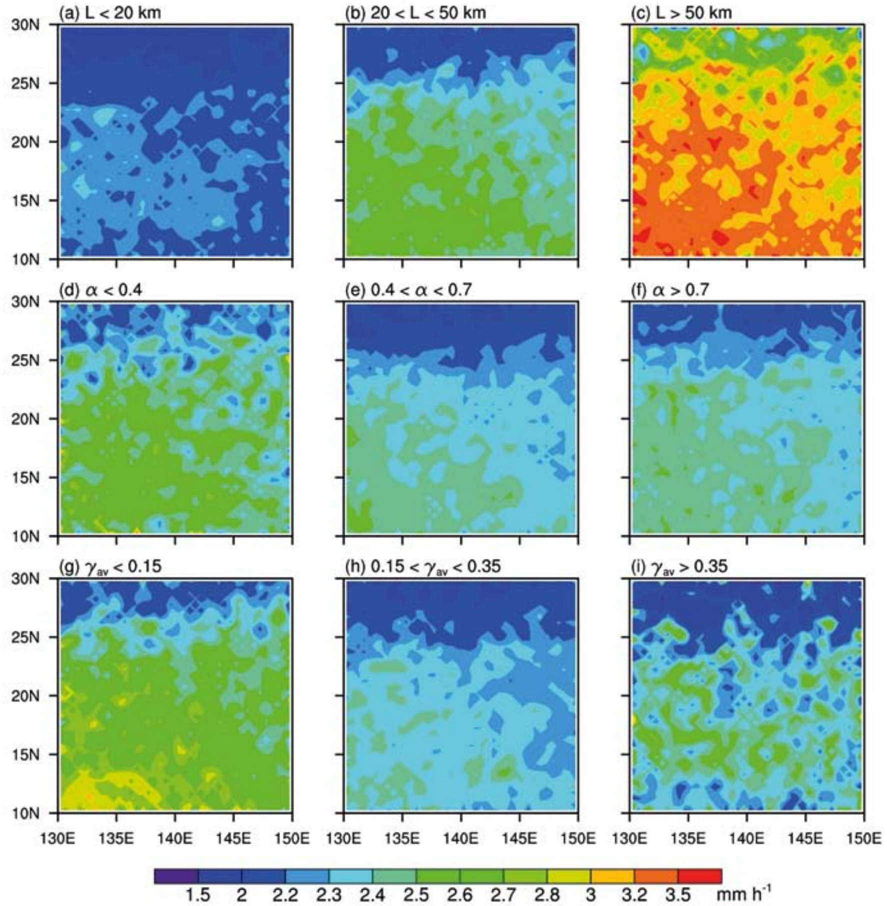

Fig. 6. Horizontal distribution of average near-surface rain rate for RCs divided by (a–c) scale L, (d–f) 2-D shape α, and 3-D shape γ_{av} over the NWP.

Based on the value of 3-D shape γ_{av}, RCs were also divided into three classes, including slender RCs with $\gamma_{av} < 0.15$, medium 3-D-shape RCs with γ_{av} between 0.15 and 0.35, and flat RCs with $\gamma_{av} > 0.35$. The horizontal distributions of their occurrence frequency are shown in Fig. 5g–5i. Over the southern portion of NWP, the ratio of slender, medium 3-D-shape, and flat RCs were 18%, 66% and 16%, relatively, while the values were relatively 30%, 60% and 10% over the northern portion.

Fig. 6g–6i shows the horizontal distributions of rainfall intensity for RCs divided by γ_{av}. The average rain rate were 2–3 mm h^{-1}, 1.5–2.5 mm h^{-1}, and 1.5–2.7 mm h^{-1} for slender, medium 3-D-shape, and flat RCs. It is showed that rainfall intensity firstly decreased sharpely and then increased slowly with increasing γ_{av}, which is consistent with Chen et al. (2021) on Tibetan Plateau. The slender RCs had the heaviest rainfall intensity while the medium 3-D-shape RCs had the weakest rainfall intensity.

4 Conclusion and discussions

The morphological features of oceanic RCs and their impact on rainfall intensity remain unclear. Using 15-year TRMM PR observations, we investigated this issue over the NWP, which is the warmest ocean over the world. The scale, 2-D shape, and 3-D shape of RCs were studied using quantitative parameters. The main conclusions are summarized as below.

The horizontal scale of RCs was described using the length of the minimum bounding rectangle (L). In the NWP, RC frequency generally decreased with L. There were about 50% RCs with L smaller than 20 km, while only 10% RCs with L larger than 50 km. Rainfall intensity increased with L, which agrees to the previous studies in other regions (Fu et al. 2020).

The 2-D shape of RCs (α) was described using the ratio of width (W) to length (L) of the minimum bounding rectangle. In the NWP, The PDF of α peaked at 0.6 with a value of 8%. Narrow RCs had the heaviest rain rate, followed by wide RCs, and the weakest for medium 2-D-shape RCs. The relationships between α and rainfall intensity were quite different from the Tibetan Plateau, where narrow RCs had the weakest precipitation (Chen et al. 2021). These regional differences highlighted the importance of regional studies.

The 3-D shape of RCs (γ_{av}) was described as the ratio of average echo-top height to the mean of L and W. In the NWP, γ_{av} ranged from 0 to 0.8 with a peak at 0.2. The average rain rate were 2–3 mm h^{-1}, 1.5–2.5 mm h^{-1}, and 1.5–2.7 mm h^{-1} for slender, medium 3-D-shape, and flat RCs. Rainfall intensity firstly decreased shapely and then increased slowly with increasing γ_{av}.

Significant zonal differences whereas less meridional differences were revealed for RCs over the NWP. RCs over the northern portion had larger scale, narrower 2-D shape, and slender 3-D shape than the southern portion. The zonal differences were attributed to two aspects. One is the higher SST over the southern portion, which promoted the occurrence of warm-cloud precipitation. The other is that the northern portion was often affected by subtropical high, thus precipitations occurred more likely to be MCS rather than warm-cloud precipitation (Chen et al. 2020).

Acknowledgments: This research was funded by the Guangdong Major Project of Basic and Applied Basic Research (grant number 2020B0301030004), the National Natural Science Foundation of China (Grant 42005062), and the Innovation Group Project of Southern Marine Science and Engineering Guangdong Laboratory (Zhuhai) (Grant number 311022006).

Data availability statement: The TRMM PR 2A25 precipitation data was collected from the Precipitation Measurement Mission website (https://pmm.nasa.gov).

References

Adler, R. F., Huffman, G. J., Bolvin, D. T., Curtis, S., & Nelkin, E. J. (2000). Tropical Rainfall Distributions Determined Using TRMM Combined with Other Satellite and Rain Gauge Information. *Journal of Applied Meteorology, 39*(12), 2007–2023. https://doi.org/10.1175/1520-0450(2001)040<2007:TRDDUT>2.0.CO;2

Barlow, M., Cullen, H., & Lyon, B. (2002). Drought in Central and Southwest Asia: La Niña, the Warm Pool, and Indian Ocean Precipitation. *Journal of Climate, 15*(7), 697–700. https://doi.org/10.1175/1520-0442(2002)015<0697:DICASA>2.0.CO;2

Basconcillo, J., Moon, I., Wang, B., & Mistry, M. (2021). Possible influence of the warm pool ITCZ on compound climate extremes during the boreal summer. *Environmental Research Letters, 16*(11), 114039. https://doi.org/10.1088/1748-9326/ac30f8

Begum, S., & Otung, I. E. (2009). Rain cell size distribution inferred from rain gauge and radar data in the UK. *Radio Science, 44*(2), 2008RS003984. https://doi.org/10.1029/2008RS003984

Capsoni, C., Fedi, F., Magistroni, C., & Paraboni, A. (1987). Data and theory for a new model of the horizontal structure of rain cells for propagation applications. *Radio Science, 22*(3), 395–404. https://doi.org/10.1029/RS022i003p00395

Chen, X., Zhou, T., Wu, P., Guo, Z., & Wang, M. (2020). Emergent constraints on future projections of the western North Pacific Subtropical High. *Nature Communications, 11*(1), 2802. https://doi.org/10.1038/s41467-020-16631-9

Chen, Y., Zhang, A., Fu, Y., Chen, S., & Li, W. (2021). Morphological Characteristics of Precipitation Areas over the Tibetan Plateau Measured by TRMM PR. *Advances in Atmospheric Sciences, 38*(4), 677–689. https://doi.org/10.1007/s00376-020-0233-1

Cornejo-Garrido, A. G., & Stone, P. H. (1977). On the Heat Balance of the Walker Circulation. *Journal of the Atmospheric Sciences, 34*(8), 1155–1162. https://doi.org/10.1175/1520-0469(1977)034<1155:OTHBOT>2.0.CO;2

Feral, L., Mesnard, F., Sauvageot, H., Castanets, L., & Lemorton, J. (2000). Rain cells shape and orientation distribution in south-west of France. *Physics and Chemistry of the Earth. Part B: Hydrology, Oceans and Atmosphere, 25*(10–12), 1073–1078. https://doi.org/10.1016/S1464-1909(00)00155-6

Fu, Y., Chen, Y., Zhang, X., Wang, Y., Li, R., Liu, Q., … Zhang, A. (2020). Fundamental Characteristics of Tropical Rain Cell Structures as Measured by TRMM PR. *Journal of Meteorological Research, 34*(6), 1129–1150. https://doi.org/10.1007/s13351-020-0035-5

Gagin, A., Rosenfeld, D., Woodley, W. L., & Lopez, R. E. (1986). Results of Seeding for Dynamic Effects on Rain-Cell Properties in FACE-2. *Journal of Climate and Applied Meteorology, 25*(1), 3–13. https://doi.org/10.1175/1520-0450(1986)025<0003:ROSFDE>2.0.CO;2

Jiang, N., & Zhu, C. (2020). Tropical Pacific cold tongue mode triggered by enhanced warm pool convection due to global warming. *Environmental Research Letters, 15*(5), 54015. https://doi.org/10.1088/1748-9326/ab7d5e

Kawamura, A., Jinno, K., Berndtsson, R., & Furukawa, T. (1996). Parameterization of rain cell properties using an advection-diffusion model and rain gage data. *Atmospheric Research, 42*(1-4), 67–73. https://doi.org/10.1016/0169-8095(95)00053-4

Kawamura, A., Jinno, K., Berndtsson, R., & Furukawa, T. (1997). Real-time tracking of convective rainfall properties using a two-dimensional advection-diffusion model. *Journal of Hydrology (Amsterdam), 203*(1–4), 109–118. https://doi.org/10.1016/S0022-1694(97)00088-7

Kumar, S., Vidal, Y., Moya-Álvarez, A. S., & Martínez-Castro, D. (2019). Effect of the surface wind flow and topography on precipitating cloud systems over the Andes and associated Amazon basin: GPM observations. *Atmospheric Research, 225*, 193–208. https://doi.org/10.1016/j.atmosres.2019.03.027

Kummerow, C., Barnes, W., Kozu, T., Shiue, J., & Simpson, J. (1998). The Tropical Rainfall Measuring Mission (TRMM) Sensor Package. *Journal of Atmospheric and Oceanic Technology, 15*(3), 809–817. https://doi.org/10.1175/1520-0426(1998)015<0809:TTRMMT>2.0.CO;2

Li, X., Sui, C. H., Adamec, D., & Lau, K. M. (1998). Impacts of precipitation in the upper ocean in the western Pacific warm pool during TOGA-COARE. *Journal of Geophysical Research, 103*(C3), 5347–5359. https://doi.org/10.1029/97JC03420

Liu, C., & Zipser, E. (2013). Regional variation of morphology of organized convection in the tropics and subtropics. *Journal of*

Geophysical Research. Atmospheres, 118(2), 453–466. https://doi.org/10.1029/2012JD018409

Luna, L. V., & Korup, O. (2022). Seasonal Landslide Activity Lags Annual Precipitation Pattern in the Pacific Northwest. *Geophysical Research Letters, 49*(18), e2022GL098506. https://doi.org/10.1029/2022GL098506

Nesbitt, S. W., Cifelli, R., & Rutledge, S. A. (2006). Storm morphology and rainfall characteristics of TRMM precipitation features. *Monthly Weather Review, 134*(10), 2702–2721. https://doi.org/10.1175/MWR3200.1

Nesbitt, S. W., Zipser, E. J., & Cecil, D. J. (2000). A Census of Precipitation Features in the Tropics Using TRMM: Radar, Ice Scattering, and Lightning Observations. *Journal of Climate, 13*(23), 4087–4106. https://doi.org/10.1175/1520-0442(2000)013<4087:ACOPFI>2.0.CO;2

Park, J., Yeh, S., & Kug, J. (2012). Revisited relationship between tropical and North Pacific sea surface temperature variations. *Geophysical Research Letters, 39*(2), 1-6. https://doi.org/10.1029/2011GL050005

Quartly, G. D. (1998). Determination of Oceanic Rain Rate and Rain Cell Structure from Altimeter Waveform Data. Part I: Theory. *Journal of Atmospheric and Oceanic Technology, 15*(6), 1361–1378. https://doi.org/10.1175/1520-0426(1998)015<1361:DOORRA>2.0.CO;2

Sauvageot, H., Mesnard, F., & Tenorio, R. S. (1999). The relation between the area-average rain rate and the rain cell size distribution parameters. *Journal of the Atmospheric Sciences, 56*(1), 57–70. https://doi.org/10.1175/1520-0469(1999)056<0057:TRBTAA>2.0.CO;2

Thatcher, L., Takayabu, Y. N., Yokoyama, C., & Pu, Z. (2012). Characteristics of tropical cyclone precipitation features over the western Pacific warm pool. *Journal of Geophysical Research, 117*(D16), 2011JD017351. https://doi.org/10.1029/2011JD017351

Tournadre, J. (1998). Determination of Rain Cell Characteristics from the Analysis of TOPEX Altimeter Echo Waveforms. *Journal of Atmospheric and Oceanic Technology, 15*(2), 387–406. https://doi.org/10.1175/1520-0426(1998)015<0387:DORCCF>2.0.CO;2

Tsonis, A. A., Triantafyllou, G. N., & Georgakakos, K. P. (1996). Hydrological applications of satellite data: 1. Rainfall estimation. *Journal of Geophysical Research, 101*(D21), 26517–26525. https://doi.org/10.1029/96JD01654

Yokoyama, C., & Takayabu, Y. N. (2012). Relationships between Rain Characteristics and Environment. Part I: TRMM Precipitation Features and the Large-Scale Environment over the Tropical Pacific. *Monthly Weather Review, 140*(9), 2831–2840. https://doi.org/10.1175/MWR-D-11-00252.1

Zhang, A., Chen, C., Chen, Y., Li, W., Chen, S., & Fu, Y. (2022a). Resilient dataset of rain clusters with life cycle evolution during April to June 2016–2020 over eastern Asia based on observations from the GPM DPR and Himawari-8 AHI. *Earth System Science Data, 14*(3), 1433–1445. https://doi.org/10.5194/essd-14-1433-2022

Zhang, A., & Fu, Y. (2018). Life Cycle Effects on the Vertical Structure of Precipitation in East China Measured by Himawari-8 and GPM DPR. *Monthly Weather Review, 146*(7), 2183–2199. https://doi.org/10.1175/MWR-D-18-0085.1

Zhang, S., Yu, Z., Wang, Y., Gong, X., Holbourn, A., Chang, F., … Li, T. (2022b). Thermal coupling of the Indo-Pacific warm pool and Southern Ocean over the past 30,000 years. *Nature Communications, 13*(1), 5457. https://doi.org/10.1038/s41467-022-33206-y

Manuscript received: October 31, 2023
Revisions requested: March 28, 2024
Revised version received: April 3, 2024
Manuscript accepted: May 15, 2024